Reaction condition optimization for non-oxidative conversion of methane using artificial intelligence

Hyun Woo Kim,[1†]* Sung Woo Lee,[2†] Gyoung S. Na,[1†] Seung Ju Han,[2] Seok Ki Kim,[2,3] Jung Ho Shin,[1] Hyunju Chang,[1]* Yong Tae Kim,[2]*

[1] Chemical Data-Driven Research Center, Korea Research Institute of Chemical Technology (KRICT), Daejeon 34114, Korea

[2] C1 Gas & Carbon Convergent Research Center, Korea Research Institute of Chemical Technology, Daejeon 34114, Republic of Korea

[3]Advanced Materials and Chemical Engineering, University of Science & Technology, Daejeon 34113, Republic of Korea

[†]*These authors contributed equally to this work.*

*E-mail address: ahwk@krict.re.kr, hjchang@krict.re.kr, ytkim@krict.re.kr

Abstract

Chemical reactions typically have numerous controllable factors that need to be optimized to yield the desired products. Although traditional experimental methods are limited to explore possible combinations of these factors, artificial intelligence (AI) can provide the optimal solution based on chemical reaction data. In this study, we optimize the non-oxidative conversion of methane to C_2 compounds using AI, such as machine learning (ML) to predict experimental results and metaheuristics to optimize reaction conditions. A decision tree-based machine learning method can reasonably predict the reaction outcomes (CH_4 conversion, C_2 yield, and selectivities for C_2 and coke) with an error of < 5%. Trained ML models are applied to maximize the C_2 yield by optimizing the reaction parameters with metaheuristics. We can simultaneously enhance the C_2 yield and suppress the coke formation by improving the multi-objective function for the optimization. We believe that our method will be helpful to optimize the chemical reaction conditions with multiple targets.

Table of Contents

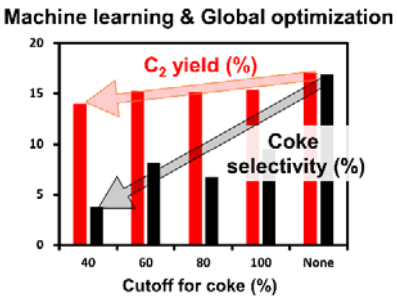

Using machine learning and global optimization, we optimize reaction conditions for non-oxidative conversion of methane.

Introduction

Numerous factors govern chemical reactions and some of the factors can be artificially manipulated to optimize the yield of desired products. In the presence of catalysts, engineering these factors for chemical reactions is required to improve the catalysts as well as reaction conditions for the best performance.[1] Due to the complexity of catalytic processes, numerous approaches have been employed, such as high-throughput methods,[2, 3] data-mining,[4-6] and genetic algorithms.[7-9] Although these approaches have been successfully applied to design new heterogeneous catalysts, machine learning (ML) methods have recently attracted considerable attention as they require smaller datasets and lower computational costs than traditional methods.[10] Moreover, in chemical reaction engineering, ML methods can play an essential role, for example, in self-optimizing platforms[11] and suggesting reaction conditions.[12]

ML can match input variables (or features) to target properties and thus can be generally employed to available datasets for numerous catalytic reactions.[4, 13-15] For example, successful applications of ML methods toward the optimization of heterogeneous catalysts are shown for a database of oxidative coupling of methane (OCM) which contains ~1800 catalysts and reaction conditions.[4] With the advancements in data science, chemical reaction data can be investigated with several approaches such as statistical analysis,[4] machine learning.[10, 16, 17] micro-kinetic simulations,[18] and meta-analysis.[19] Moreover, a recent experimental study demonstrated that the combination of high-throughput experiments and ML techniques can provide catalyst compositions with improved catalytic efficiencies for the OCM with less effort.[20, 21]

In chemistry-related fields, the developments of OCM catalysts is important as methane is abundant in natural gas[22] and is easily found in biomass.[23, 24] Considering its importance, several processes have been proposed for the activation of methane molecules, such as steam reforming,[25]

dry reforming,[26] and oxidative[27] and non-oxidative[28] coupling of methane. Recently, non-oxidative coupling of methane (NOCM) or methane to olefins, aromatics, and hydrogen (MTOAH) has attracted considerable attention[29, 30] because it does not require any oxidizing reagents, which potentially transform methane to oxidized products such as CO_2. Although undesirable oxidation reactions do not occur in MTOAH unlike OCM, the application of MTOAH is still limited as it occurs through thermodynamically unfavorable processes toward hydrocarbons.[31] Several strategies with external energy sources such as heat.[28, 32-34] photon,[35, 36] and plasma[37, 38] have been proposed to overcome this limitation.

The main challenge of MTOAH is the maximum conversion of methane possible while achieving high energy efficiency. The initial C-H bond activation of methane requires the highest energy (425 kJ mol^{-1}) among other steps. Thus, controlling the reaction pathways toward target products is quite challenging.[39] Thermodynamics favors coke formation under radical-mediated conditions, requiring a precise design of lateral active sites,[40] catalytic systems,[41] and reaction engineering.[42, 43] Experimentally, an MTOAH system facilitates numerous improvements in terms of conversion and selectivity (i.e., methane conversion of 48% and ethylene selectivity of 50% using a silica-lattice-confined single Fe atom).[30] However, the lack of theoretical understanding may hinder the development of breakthrough technologies in this field. According to our previous study, although the MTOAH reaction is dominated in the gas phase, a proper use of the catalytic surface can improve the reaction activity toward the efficient formation of the hydrocarbon products.[29]

To maximize the yield of the desired product in the MTOAH reaction proceeding at a high temperature, it is necessary to simultaneously consider the catalytic reaction[44] and gas-phase radical reaction. However, despite the significant contribution of the gas-phase reaction to the

product distribution, no chemical method, other than changing operation conditions, has been reported to control its kinetics. Moreover, as the gas-phase reaction is a set of numerous radical chain reactions, it is almost impossible to determine the optimal reaction conditions by simulating each individual reaction. Therefore, it is essential to accumulate information on gas-phase methane pyrolysis and optimize operating conditions for further improvement of the catalytic system.

To this end, we employed a hybrid approach by combining supervised ML models and metaheuristics-based optimizations[45] to enhance the MTOAH to C_2 molecules. Adopting an idea that artificial intelligence (AI) is a broad concept, which includes machine learning,[46] we will shortly denote our hybrid approach as an AI method. Experimentally, we chose a quartz tubular reactor with a crystalline SiO_2 surface, which can balance gas-phase reactions. We then constructed ML models to predict experimental results. A decision tree–based method[47] could reasonably predict the reaction outcomes (CH_4 conversion, C_2 yield, and selectivities for C_2 and coke) with an error of < 5%. After establishing ML models, we maximized the C_2 yield by optimizing the experimental input variables using metaheuristics.[45] We also experimentally demonstrated that the C_2 yield can be enhanced without increasing the coke formation with AI acting as a guide. We believe that our method can be useful for optimizion of chemical reaction conditions with multiple targets.

Methods

Experiment

MTOAH was carried out in a quartz tubular reactor (length = 150 cm) with various inner diameters in which the fluid moves horizontally. The reactor achieved a uniform temperature profile by connecting three different furnaces in series to a heating zone (45 cm). Each reactor was controlled

by six SiC heating elements monitored by three R-type thermocouples in direct contact with the outer surface of the tubular reactor. The reactivity of methane in the space between the furnaces was negligible. For safe operation, the system was installed in a container where negative pressure was maintained and could automatically shut off in case of gas leaks and pressure changes. The reactor reached the reaction temperature at a flow rate of 100 mL min^{-1} using He at a ramping rate of 10°C min^{-1}. Methane and methane/hydrogen gas containing Ar as an internal standard were then fed into the reactor using mass flow controllers (5850E, Brooks®). All gases were passed through an oxygen/moisture trap (OT3-4, Agilent) before they were fed into the system to remove O_2 and H_2O. To impede the condensation of aromatics, all lines from the reactor to the online gas chromatograph (GC) were heated to 190 °C, and additional H_2 was supplied to dilute the gas effluent from the reactor. We installed a 500 mL gas-solid separator and particle filters behind the reactor to prevent it from clogging due to coke. The gas analysis was carried out using an online GC (7820A, Agilent) equipped with two blocks of detectors composed of a thermal conductivity detector (TCD) and flame ionization detectors (FIDs). The molar concentrations of H_2, CH_4, Ar, CO, CO_2, and C2 (ethane, ethylene, and acetylene) components were determined by the TCD with a ShinCarbon ST column (Restek Corp., Catalog No. 80486-800). The injection port and detector were maintained at 250°C and 200°C, respectively. The column flow rate of the He carrier gas was 30 mL min^{-1}. C3–C4 hydrocarbons and aromatics including benzene, naphthalene, and alkyl aromatics (toluene, xylenes, etc.) were separated using an Rtx-VMS column (Restek Corp., Catalog No. 49915). Their concentrations were measured using the FID. The injection port and detector were maintained at 200°C and 250°C, respectively. The column flow rate of the He carrier gas was 0.5 mL min^{-1}. The GC oven temperature regime started off with a constant temperature

of 50°C for 6 min, followed by an increase to 200°C at 15°C min^{-1}, and finally maintained a constant temperature of 200°C for 8 min.

The methane conversion was calculated as mole ratio of reacted methane to methane fed into the system. The product selectivity was calculated by the carbon amount of the product (mol) divided by the carbon amount of the reacted methane (mol). We calculate the coke selectivity according to the carbon balance at which the sum of the product selectivities detected by GC was subtracted from 100%. The product yield was calculated by dividing the carbon amount (mol) of the product by the amount of fed methane (mol). These experimental results were tabulated in ESI (see Table S1).

Target property prediction with ML

To apply the ML approach, we reorganized the experimental data with six input variables and four target values. The input variables included (1) pressure (p), (2) temperature (T), (3) flow rate (f), (4) H_2 content (H_2), and (5) length (l_R) and (6) diameter (d_R) of the reactors. The four target values were the (1) C_2 yield, (2) C_2 selectivity, (3) CH_4 conversion, and (4) coke selectivity. After preparing the experimental data for the training of the ML models, we generated two ML models based on different algorithms such as fully-connected neural network (FNN)[46, 48] and XGBoost (abbreviated as XGB in this paper).[47] In fact, FNN and XGB are used in various the chemistry-related areas.[49] FNN was employed as implemented in Tensorflow,[50] while XGB was used as present in the XGBoost python package. By using the five-fold cross-validation, we searched the optimal hyperparameters of FNN by varying three factors: activation function, number of nodes, and optimizer. These parameters are listed in Table S2 in ESI. Scanning of possible combinations of hyperparameters showed that the combination of Sigmoid function, 60 nodes for two hidden

layers, and Adadelta optimizer[51] provided the best performance in the training of the FNN model for the prediction of the C_2 selectivity. We targeted the C_2 selectivity in hyperparameter optimization as it showed the largest error as shown later. We also performed the hyperparameter optimization for XGB models and selected 300 estimators and a maximum depth of 5. The range of the number of estimators and depth considered in this work are also listed in Table S2. For all cases, 80% of the experimental data were used as the training set to optimize model parameters, while the rest were treated as the test set for evaluations. Here, we randomly selected data for training and test sets and listed indices of test set (see Table S3 in ESI) as splitting training set and test set can influence the performance of the ML model.

Global optimization with metaheuristics

Metaheuristics is a widely used mathematical optimization method to find the optimal solution of a complex black-box model such as deep road networks,[52] neural networks,[53] and materials discovery,[54, 55] In this work, we adopted the artificial bee colony (ABC)[53] algorithm as a representative example of metaheustrics, which had been verified in several benchmarks[56] and applied to various fields.[57] Figure 1 depicts the overall optimization process of the ABC algorithm, consisting mainly of four steps as follows: (1) Initial feature vectors (or population) are randomly generated based on a random seed, (2) each feasible solution is evaluated by the trained ML model and penalty function, (3) feasible solutions for the next trial are generated according to the algorithm-specific rules and solutions scored at the current stage, and finally (4) if the user-defined termination condition is satisfied, the optimization is terminated and the solution with the best score is returned. We repeated these optimization cycles 1000 times. The size of population was set to 100. Notably, the optimization reached the converged solution after ~100 optimization cycles.

Results and Discussion

The MTOAH was performed in a tubular quartz reactor with a crystalline surface as shown in Fig. 2 and Table S1. The methane conversion in the tubular reactor occurred through four main reaction steps:[58] (1) initial activation of the C−H bond in methane, (2) conversion of methyl radicals to ethane and subsequent dehydrogenations, (3) C−C coupling of C_2 species to aromatics, and (4) subsequent reactions for coke formation. Each reaction step is largely dependent on the concentration of unstable radicals, which can only remain for a period of microseconds in the reaction system.[58] The SiO_2 surface of the tubular reactor not only activates the C−H bond of methane, but also acts as a coke terminator for unsaturated hydrocarbons.[29] We adjusted several reaction parameters to change the free energies of the reaction, such as the temperature (890–1200 °C), pressure (0.005–0.888 barg) and the reactant flow rate (40–320 mL min^{-1}), reactor diameter (4–16 mm), and reactor length (15–45 cm). To improve the stability of unsaturated hydrocarbons during the entire reaction, we varied the H_2 content in the feed, which was calculated as the mole ratio of H_2 to CH_4 and Ar. The yield of hydrocarbons was not thermodynamically limited. Only the C_2 distribution of ethane, ethylene, and acetylene was near the equilibrium. Notably, the C_2 selectivity altered by the reaction parameter tended to be inversely proportional to the coke selectivity. According to our experimental data used in this study, the quartz reactor achieved a C_2 yield of 15.7 %; however, coke selectivity of 27.7% was observed as well (Table S1, Index 245). We found that by keeping the C_2 yield in a parametric way, we systematically reduced the coke selectivity to 10.4% (Table S1, Index 249). To further improve the C_2 yield, individual parameters must define their role. Therefore, ML is suitable for logically designing optimal operation conditions.

Before the application of AI methods, we briefly analyzed the experimental data. As shown in Fig. 2, we visualized four important experimental quantities: C_2 yield, C_2 selectivity, CH_4 conversion, and coke selectivity. As we focused on enhancing the C_2 yield, a total of 250 experimental data were collected, and categorized into five groups according to the C_2 yield in ascending order. We assigned indices to these data. Thus, index 250 is the experimental result with the highest C_2 yield, while index 1 corresponds to the lowest C_2 yield. Fig. 2 shows that the C_2 yield varied in the range of ~0 to ~15%. Complex relationships were observed between other quantities and these indices. We analyzed the C_2 yield, according to the input variables such as (1) pressure, (2) temperature, (3) flow rate, (4) H_2 content, and (5) length and (6) diameter of the reactor, as shown in Fig. 3. Out of these, only temperature was weakly related to the C_2 yield, which was almost independent of the other experimental input variables. Therefore, we can expect that ML methods can be used to determine the complex relationships between the experimental input and output variables.

In Fig. 4, the ML models based on FNN and XGB predicted the experimental results within a mean absolute error (MAE) of 5%. Overall, XGB provides better prediction results than FNN. As it is challenging to generate high-quality experimental data for a specific purpose, the applicability of XGB to the small dataset generated from our experimental results is valuable. With these, we adopted XGB for the further analysis in this work and displayed prediction results for four target quantities as shown in Fig. 5. We can explain relatively large MAEs for C_2 and coke selectivities based on several outliers in the prediction of these quantities, depicted in Fig. 5(b) and 5(d). In addition, XGB can rank input features based on their relative importance in the construction of the ML as shown in Fig. 6. This is a valuable characteristic of XGB because it records the contribution of each feature during the training step, unlike the typical FNN. The

reaction temperature is the most important variable in the prediction of C_2 yield as the temperature was roughly related to the C_2 yield as shown in Fig. 3(b). Other variables also participated to improve the XGB model. Their relative importance values ranged between 5 – 20%. The relative contributions of the temperature and pressure are different for MTOAH and OCM as the pressure exhibits the highest importance among several experimental parameters of OCM.[17] For the C_2 and coke selectivities, pressure was chosen as the most important factor among the input variables although the C_2 selectivity is also considerably affected by the flow rate and H_2 content. According to relative importances from the XGB algorithm, the prediction of methane conversion was mostly influenced by the flow rate. By comparing the contributions of each input variable, we can propose a simple guide to optimize the reaction conditions for MTOAH as the modulation of temperature and pressure is important to increase the C_2 yield and C_2 selectivity, respectively.

We employed the metaheuristics-based optimization to evaluate the experimental conditions for maximum C_2 yield. As explained above, the optimization algorithm utilizes the trained XGB model to predict MTOAH results based on our experimental data. During the optimization, we restricted the range of experimental input parameters such as temperature (850–1250 °C), pressure (0–1 barg), the reactant flow rate (10–350 mL min^{-1}), the H_2 content (0–5.5), reactor diameter (3–18 mm), and reactor length (10–50 cm). These ranges of parameters are experimentally feasible as they are ~ 10% beyond the parameters that were used in the data generation. Notably, the algorithm proposes a feasible solution based on AI without relying on additional experiments. Figure 7 shows XGB-model-based predicted values for the C_2 yield and coke selectivity under the optimized experimental conditions. The x-axis represents the number of data. We show the maximum and average values of the experimental data for each case. For the coke selectivity, it is meaningless to show the maximum because the value was larger than 80%

even with the first 50 experimental data. As we reorganized experimental data based on the C_2 yield in ascending order, the C_2 yield increased with the number of data. Therefore, training the XGB model with more and more data means that the data with higher C_2 yield is used for training. The results obtained with the XGB models with different numbers of experimental data were varied. For all tested cases, our AI-based optimization improved the C_2 yield from 8.03% to 18.10% when compared with the maximum C_2 yield obtained by experiments. However, the formation of coke, a by-product of MTOAH, also increased with the increase in the C_2 yield.

The ideal optimization should maximize the yield of C_2 compounds and their selectivity, and thus minimize the selectivity for the coke. The optimization of multiple target quantities is an important issue in catalytic reaction engineering.[59, 60] We devised a set of scoring functions by taking the geometric mean of linear functions of three quantities, which are CH_4 conversion, C_2 selectivity, and coke selectivity. These linear functions have been shown in Fig. 8. It should be noted that there coule be enumorous possibilities to construct scoring functions and we selected one of them. Here, we use the C_2 selectivity, as a high C_2 selectivity is roughly related to a low coke selectivity. The yield of C_2 compounds and their selectivities were scored linearly from 0 to 1. For the coke selectivity, we approached in the opposite way and introduced a cutoff. If the coke selectivity becomes higher than the cutoff, the score is set to 0. We tested four cutoffs for the coke selectivity as shown in Fig. 8(b). Using these, we could change the optimization of three target quantities to that of a single quantity called the scoring function. Our aim is to maximize the value of these functions instead of the C_2 yield because they enable us to consider the C_2 yield and coke selectivity simultaneously. Figure 9 shows the C_2 yield and coke selectivity obtained by optimizing the scoring functions. These results support the finding that a reduction in the cutoff increases the penalty for the coke formation. Therefore, the AI can find the experimental conditions to optimize

the C_2 yield with a smaller amount of coke formation. When the cutoff for the coke was 40%, the XGB model predicted a C_2 yield of 13.97% and coke selectivity of 3.76%. As the MAE of the coke selectivity was 2.78%, the coke selectivity already reached the prediction limit in this case and we could not reduce the cutoff below 40%. This experimental condition was further used to validate our AI approach with an additional MTOAH experiment, as shown in Table 1. Although some mismatches in experimental variables existed in practice, we could achieve a C_2 yield of 10.52% with a low coke selectivity of 1.10%. Five cases (Indices of 172, 175, 184, 186, and 188) in Table S1 show similar C_2 yields to this results, but the coke selectivities were 3.2–4.8% in these cases, which were higher than the experimental values in Table 1. We also tabulated these experimental data in Table S4 in ESI. In our experiment, 73 practices provided C_2 yields above 10.52%; however, they mostly exhibited coke selectivity above 6%. Considering the prediction errors of ML models (~3% in this study), we confirm that AI suggestions can predict experimental conditions with better results. As quantifying the uncertainty from ML prediction is an active research topic,[61, 62] quantitative error analysis could be helpful for improving AI suggestions in the future. From the experimental perspective, with this Al's reasonable prediction, we expect that complex reaction mechanisms of MTOAH will be further optimized with cascade reactors containing different parameters for better C_2 yield as well as C_2H_4 yield while maintaining negligible coke selectivity. Furthermore, it is also necessary to develop AI approaches and accumulate refined data for more accurate ML models, which can enhance AI suggestions to improve catalytic processes such as MTOAH for application in the chemical industry.

Table 1. Experimental conditions and outcomes of the AI suggestion and additional experiment.

	p (barg)	T (°C)	f (sccm)	H_2 content	l_R (cm)	d_R (mm)	C_2 yield (%)	Coke selectivity (%)
AI	0.16	1196.3	148.7	3.6	10.6	6.4	13.97	3.76
Exp.	0.13	1196.3	148.8	3.6	15.0	6.5	10.52	1.10

Conclusions

In summary, we propose an AI approach to optimize the MTOAH reaction to C_2 compounds using ML for regression and metaheuristics for global optimization. We experimentally generated MTOAH data and then applied two well-known ML methods, XGB and FNN. As these ML models can predict the experimental results with errors of < 5% and XGB works better than FNN, we further employed the trained XGB models. In addition, we can take advantage of using XGB models as they can provide a qualitative guideline for better experimental results based on the relative importance of the input variables. We can also propose the experimental conditions for enhancing the C_2 yield in a quantitiative manner by adopting ABC algorithm, which is a metaheuristic method. However, we observed that focusing on the C_2 yield only will increase the production of the coke, a side product in this work. To optimize both C_2 yield and the coke selectivity at the same time, we devised scoring functions and found experimental conditions suggested by ABC algorithm. We experimentally verified that the suggested condition can indeed provide a reasonable C_2 yield with a low coke selectivity. With these, we believe that our approach can be applied to optimize various chemical reactions in the future.

Acknowledgments
This research was financially supported by C1 Gas Refinery Program through the National Research Foundation of Korea (NRF) funded by the Ministry of Science, ICT and Future Planning (NRF-2017M3D3A1A01037001). This study was also supported by a core Korea Research Institute of Chemical Technology (KRICT) project (SI2051-10).

References

1. J. Hagen, *Industrial catalysis: a practical approach*, John Wiley & Sons, 2015.
2. R. J. Hendershot, C. M. Snively and J. Lauterbach, *Chem. Eur. J.*, 2005, **11**, 806-814.
3. D. Farrusseng, *Surf. Sci. Rep.*, 2008, **63**, 487-513.
4. U. Zavyalova, M. Holena, R. Schlögl and M. Baerns, *ChemCatChem*, 2011, **3**, 1935-1947.
5. E. Kim, K. Huang, A. Saunders, A. McCallum, G. Ceder and E. Olivetti, *Chem. Mater.*, 2017, **29**, 9436-9444.
6. G. Rothenberg, *Catal. Today*, 2008, **137**, 2-10.
7. T. C. Le and D. A. Winkler, *Chem. Rev.*, 2016, **116**, 6107-6132.
8. J. E. Kreutz, A. Shukhaev, W. Du, S. Druskin, O. Daugulis and R. F. Ismagilov, *J. Am. Chem. Soc.*, 2010, **132**, 3128-3132.
9. S. Moehmel, N. Steinfeldt, S. Engelschalt, M. Holena, S. Kolf, M. Baerns, U. Dingerdissen, D. Wolf, R. Weber and M. Bewersdorf, *Appl. Catal. A*, 2008, **334**, 73-83.
10. K. Suzuki, T. Toyao, Z. Maeno, S. Takakusagi, K. i. Shimizu and I. Takigawa, *ChemCatChem*, 2019, **11**, 4537-4547.
11. A. D. Clayton, A. M. Schweidtmann, G. Clemens, J. A. Manson, C. J. Taylor, C. G. Niño, T. W. Chamberlain, N. Kapur, A. J. Blacker, A. A. Lapkin and R. A. Bourne, *Chem. Eng. J.*, 2020, **384**, 123340.
12. H. Gao, T. J. Struble, C. W. Coley, Y. Wang, W. H. Green and K. F. Jensen, *ACS Cent. Sci.*, 2018, **4**, 1465-1476.
13. M. E. Günay and R. Yildirim, *ChemCatChem*, 2013, **5**, 1395-1406.
14. Ç. Odabaşı, M. E. Günay and R. Yıldırım, *Int. J. Hydrog. Energy*, 2014, **39**, 5733-5746.

15. M. Baysal, M. E. Günay and R. Yıldırım, *Int. J. Hydrog. Energy*, 2017, **42**, 243-254.

16. J. Ohyama, S. Nishimura and K. Takahashi, *ChemCatChem*, 2019, **11**, 4307-4313.

17. K. Takahashi, I. Miyazato, S. Nishimura and J. Ohyama, *ChemCatChem*, 2018, **10**, 3223-3228.

18. L. Pirro, P. S. Mendes, B. D. Vandegehuchte, G. B. Marin and J. W. Thybaut, *React. Chem. Eng.*, 2020, **5**, 584-596.

19. R. Schmack, A. Friedrich, E. V. Kondratenko, J. Polte, A. Werwatz and R. Kraehnert, *Nat. Commun.*, 2019, **10**, 441.

20. T. N. Nguyen, T. T. P. Nhat, K. Takimoto, A. Thakur, S. Nishimura, J. Ohyama, I. Miyazato, L. Takahashi, J. Fujima and K. Takahashi, *ACS Catal.*, 2019, **10**, 921-932.

21. I. Miyazato, S. Nishimura, L. Takahashi, J. Ohyama and K. Takahashi, *J. Phys. Chem. Lett.*, 2020, **11**, 787−795.

22. S. Faramawy, T. Zaki and A.-E. Sakr, *J. Nat. Gas Sci. Eng.*, 2016, **34**, 34-54.

23. M. Montingelli, S. Tedesco and A. Olabi, *Renew. Sust. Energy Rev.*, 2015, **43**, 961-972.

24. R. Chandra, H. Takeuchi and T. Hasegawa, *Renew. Sust. Energy Rev.*, 2012, **16**, 1462-1476.

25. A. Iulianelli, S. Liguori, J. Wilcox and A. Basile, *Catal. Rev.*, 2016, **58**, 1-35.

26. N. A. K. Aramouni, J. G. Touma, B. A. Tarboush, J. Zeaiter and M. N. Ahmad, *Renew. Sust. Energy Rev.*, 2018, **82**, 2570-2585.

27. J. H. Lunsford, *Angew. Chem. Int. Ed.*, 1995, **34**, 970-980.

28. Y. Xu, X. Bao and L. W. Lin, *J. Catal.*, 2003, **216**, 386-395.

29. S. J. Han, S. W. Lee, H. W. Kim, S. K. Kim and Y. T. Kim, *ACS Catal.*, 2019, **9**, 7984-7997.

30. X. Guo, G. Fang, G. Li, H. Ma, H. Fan, L. Yu, C. Ma, X. Wu, D. Deng and M. Wei, *Science*, 2014, **344**, 616-619.

31. P. Tang, Q. Zhu, Z. Wu and D. Ma, *Energy Environ. Sci.*, 2014, **7**, 2580-2591.

32. H. Amariglio, J. Saint-Just and A. Amariglio, *Fuel Process. Technol.*, 1995, **42**, 291-323.

33. L. Guczi, K. Sarma and L. Borkó, *Catal. Lett.*, 1996, **39**, 43-47.

34. H. Sheng, E. P. Schreiner, W. Zheng and R. F. Lobo, *ChemPhysChem*, 2018, **19**, 504-511.

35. F. Amano, C. Akamoto, M. Ishimaru, S. Inagaki and H. Yoshida, *Chem. Commun.*, 2020, **56**, 6348-6351.

36. X. Yu, V. L. Zholobenko, S. Moldovan, D. Hu, D. Wu, V. V. Ordomsky and A. Y. Khodakov, *Nat. Energy*, 2020, 1-9.

37. J. Kim, J. Jeoung, J. Jeon, J. Kim, Y. S. Mok and K.-S. Ha, *Chem. Eng. J.*, 2019, **377**, 119896.

38. M. Scapinello, E. Delikonstantis and G. D. Stefanidis, *Chem. Eng. Process.*, 2017, **117**, 120-140.

39. A. Holmen, *Catal. Today*, 2009, **142**, 2-8.

40. P. Xie, T. Pu, A. Nie, S. Hwang, S. C. Purdy, W. Yu, D. Su, J. T. Miller and C. Wang, *ACS Catal.*, 2018, **8**, 4044-4048.

41. Y. Xiao and A. Varma, *ACS Catal.*, 2018, **8**, 2735-2740.

42. S. C. Oh, E. Schulman, J. Zhang, J. Fan, Y. Pan, J. Meng and D. Liu, *Angew. Chem.*, 2019, **131**, 7157-7160.

43. M. Sakbodin, Y. Wu, S. C. Oh, E. D. Wachsman and D. Liu, *Angew. Chem.*, 2016, **128**, 16383-16386.

44. S. K. Kim, H. W. Kim, S. J. Han, S. W. Lee, J. Shin and Y. T. Kim, *Commun. Chem,*, 2020, **3**, 58.

45. Z. Beheshti and S. M. H. Shamsuddin, *Int. J. Adv. Soft Comput. Appl*, 2013, **5**, 1-35.

46. I. Goodfellow, Y. Bengio and A. Courville, *Deep learning*, MIT press, 2016.

47. T. Chen and C. Guestrin, 2016.

48. Y. LeCun, Y. Bengio and G. Hinton, *Nature*, 2015, **521**, 436-444.

49. Z. Wu, B. Ramsundar, E. N. Feinberg, J. Gomes, C. Geniesse, A. S. Pappu, K. Leswing and V. Pande, *Chem. Sci.*, 2018, **9**, 513-530.

50. M. Abadi, P. Barham, J. Chen, Z. Chen, A. Davis, J. Dean, M. Devin, S. Ghemawat, G. Irving and M. Isard, 2016.

51. M. D. Zeiler, *arXiv preprint arXiv:1212.5701*, 2012.

52. S. B. Jha, J. Jha and M. K. Tiwari, *Comput. Ind. Eng.*, 2019, **130**, 166-186.

53. D. Karaboga, B. Akay and C. Ozturk, 2007.

54. P. C. Jennings, S. Lysgaard, J. S. Hummelshøj, T. Vegge and T. Bligaard, *npj Comput. Mater.*, 2019, **5**, 46.

55. S. Wu, Y. Kondo, M.-a. Kakimoto, B. Yang, H. Yamada, I. Kuwajima, G. Lambard, K. Hongo, Y. Xu and J. Shiomi, *npj Comput. Mater.*, 2019, **5**, 66.

56. D. Karaboga and B. Akay, *Appl. Math. Comput.*, 2009, **214**, 108-132.

57. D. Karaboga, B. Gorkemli, C. Ozturk and N. Karaboga, *Artif. Intell. Rev.*, 2014, **42**, 21-57.

58. A. Holmen, O. Olsvik and O. Rokstad, *Fuel Process. Technol.*, 1995, **42**, 249-267.

59. C. Mateos, M. J. Nieves-Remacha and J. A. Rincón, *React. Chem. Eng.*, 2019, **4**, 1536-1544.

60. A. D. Clayton, J. A. Manson, C. J. Taylor, T. W. Chamberlain, B. A. Taylor, G. Clemens and R. A. Bourne, *React. Chem. Eng.*, 2019, **4**, 1545-1554.

61. A. A. Peterson, R. Christensen and A. Khorshidi, *Phys. Chem. Chem. Phys.*, 2017, **19**, 10978-10985.

62. J. P. Janet, C. Duan, T. Yang, A. Nandy and H. J. Kulik, *Chem. Sci.*, 2019, **10**, 7913-7922.

Figures

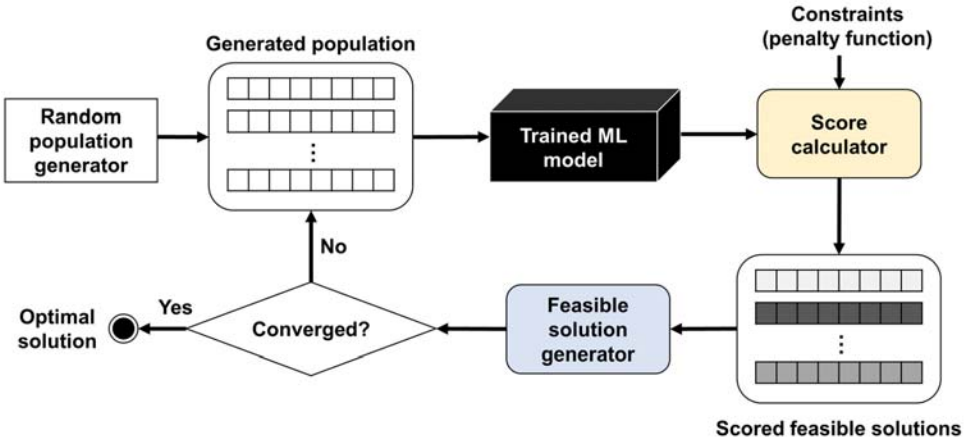

Figure 1. Schematic of the metaheuristic optimization.

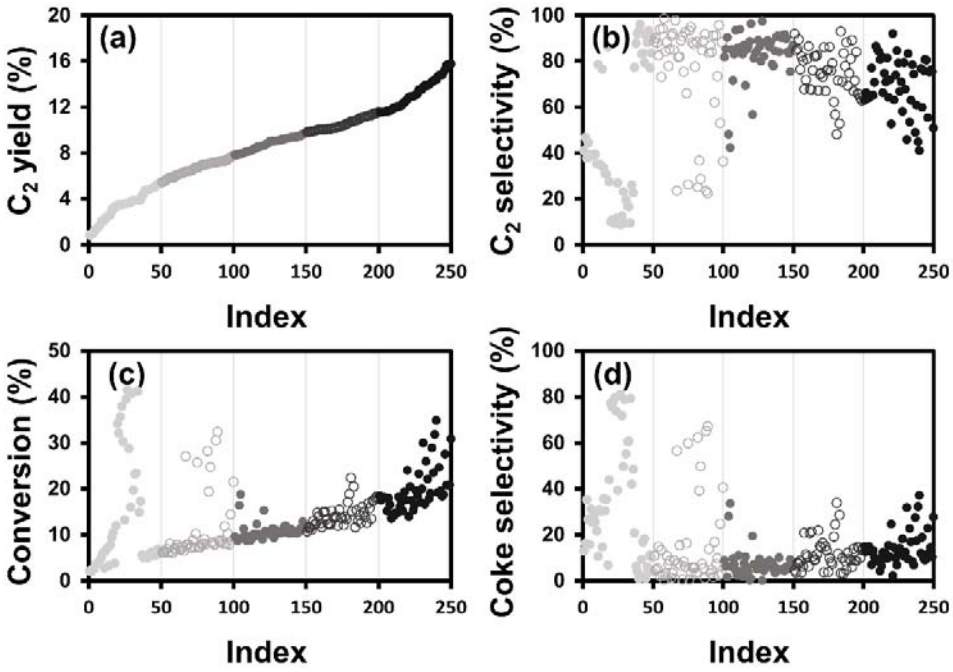

Figure 2. Distribution of experimental data for the (a) C_2 yield, (b) C_2 selectivity, (c) CH_4 conversion, and, (d) coke selectivity. We classified the data for C_2 yield into five groups in ascending order. Grouped data with higher yields are shown by darker colors.

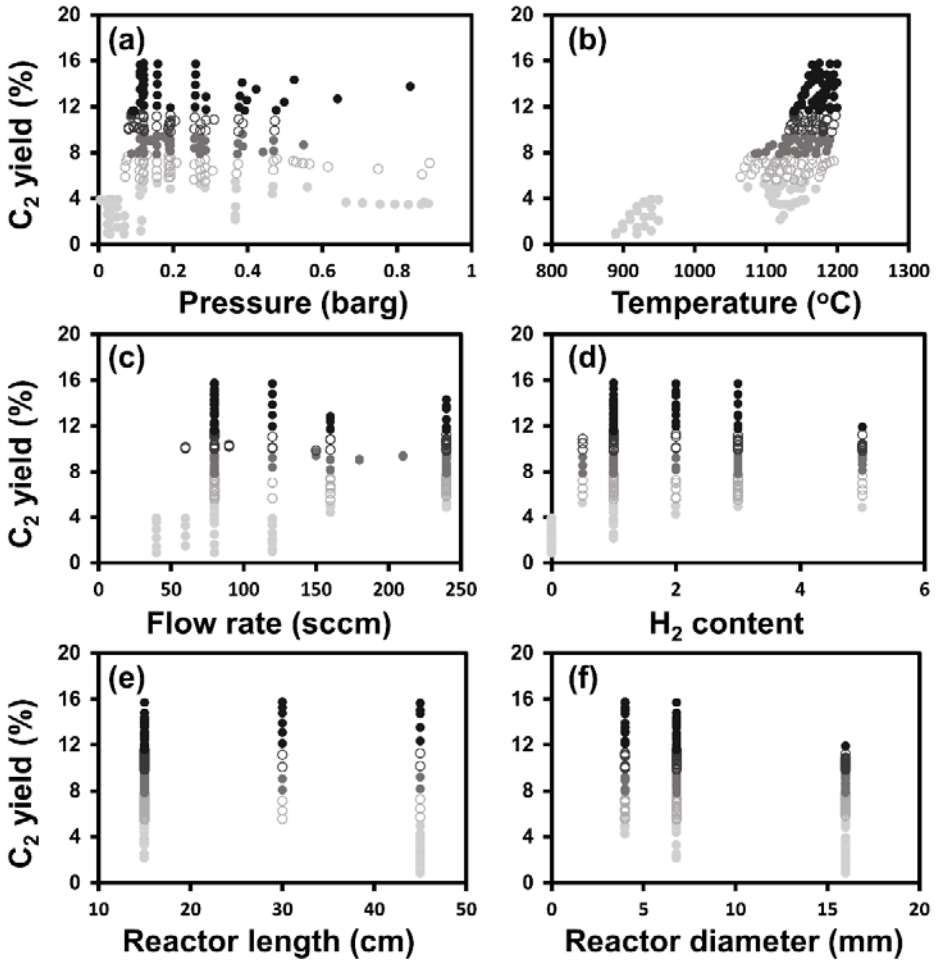

Figure 3. Experimental input parameters for C_2 yield. The color scheme is the same as in Fig. 2.

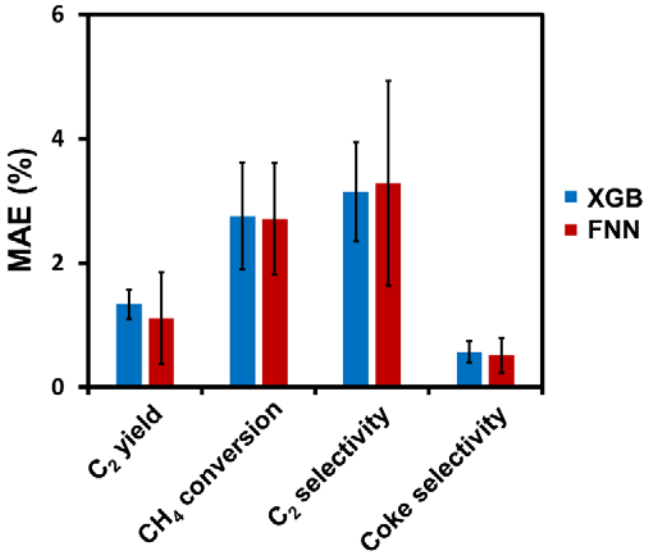

Figure 4. Prediction errors of the two ML models (XGB and FNN) for the experimental results: C_2 yield, CH_4 conversion, C_2 selectivity, and coke selectivity. We measured the prediction error five times by changing the number of data by 50, from 50 to 250. The average of these errors and their standard deviation are displayed.

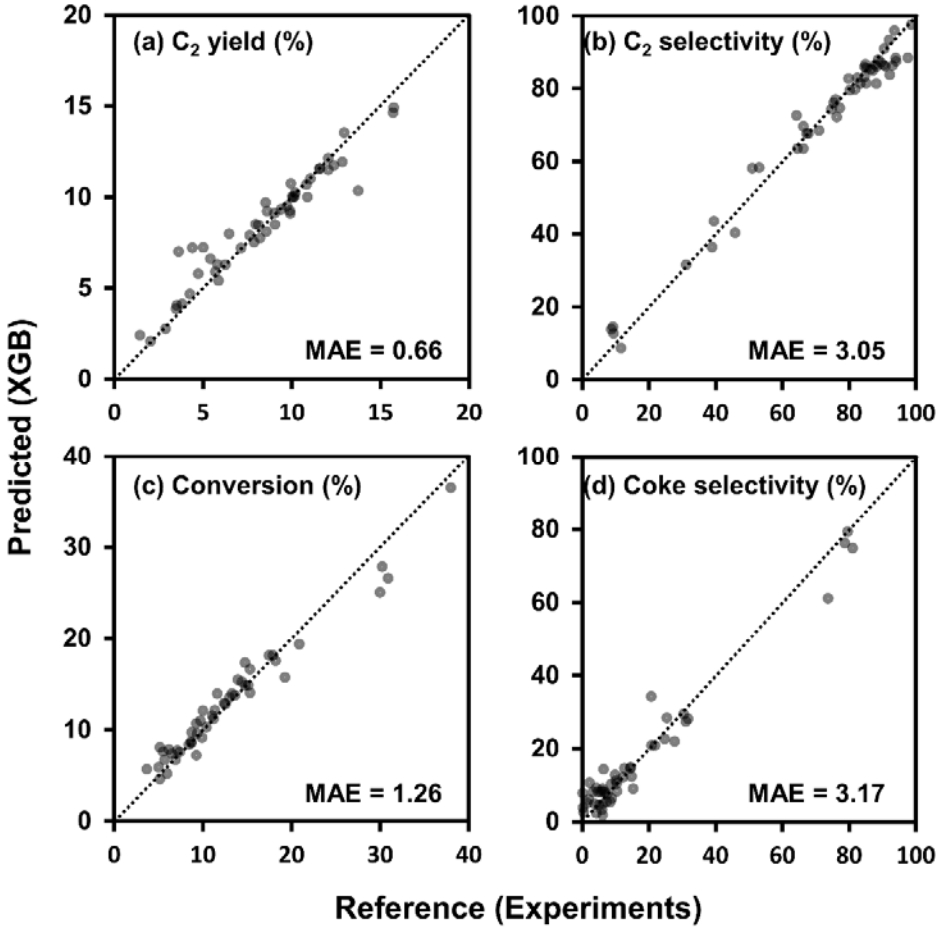

Figure 5. Comparison of the predicted and reference data with corresponding MAE for (a) C_2 yield, (b) C_2 selectivity, (c) CH_4 conversion, and (d) coke selectivity.

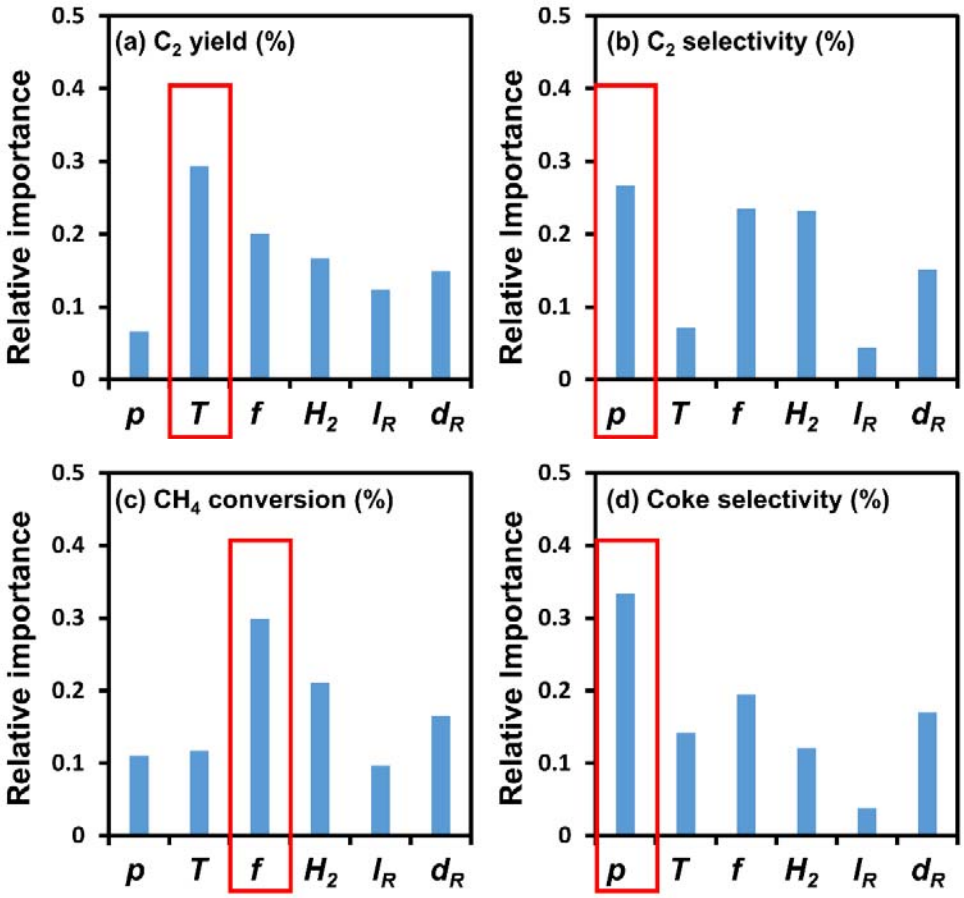

Figure 6. Relative importance values of the experimental input variables used for building ML models to predict the (a) C_2 yield, (b) C_2 selectivity, (c) CH_4 conversion, and (d) coke selectivity. The most important variable is highlighted with a red box.

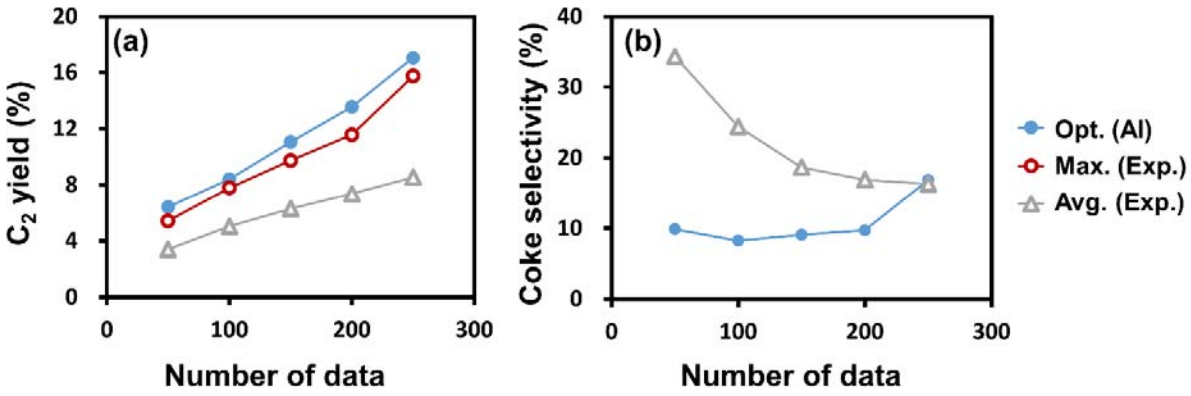

Figure 7. Results of the AI-based optimization and experiments for the (a) C_2 yield and (b) coke selectivity. The AI optimization results (filled blue circles) are compared to the maximum value of the experimental results (open red circles) and their average (open gray triangles).

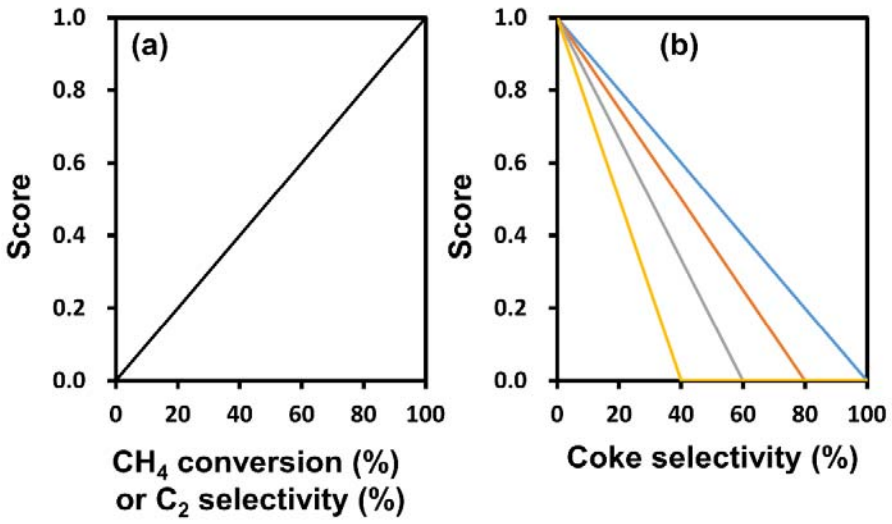

Figure 8. Scoring functions for the (a) CH_4 convsersion and C_2 selectivity and (b) coke selectivity. In (b), the cutoff values for the coke selectivity are set to 40% (yellow), 60% (gray), 80% (orange), and 100% (blue).

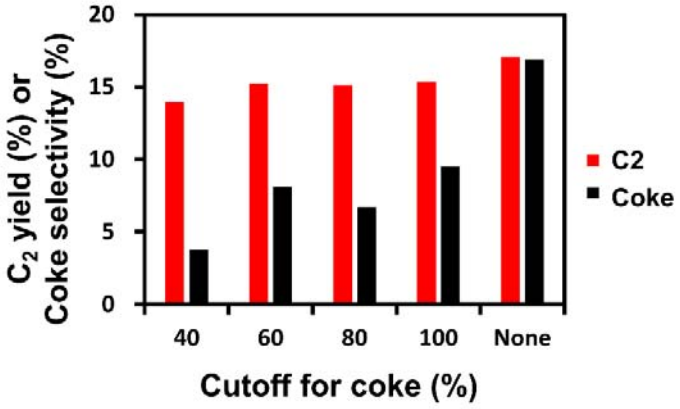

Figure 9. Effects of the cutoff for coke selectivity on the C_2 yield (red) and coke selectivity (black).